LANGMUIR Article
Cite This: Langmuir 2018, 34, 15495−15506
pubs.acs.org/Langmuir

Effect of Formulation and Processing Parameters on the Size of mPEG-*b*-p(HPMA-Bz) Polymeric Micelles

Mahsa Bagheri,[†,▽] Jaleesa Bresseleers,[‡,§,▽] Aida Varela-Moreira,[†,∥] Olivier Sandre,[⊥] Silvie A. Meeuwissen,[‡] Raymond M. Schiffelers,[∥] Josbert M. Metselaar,[#] Cornelus F. van Nostrum,[†] Jan C. M. van Hest,[§] and Wim E. Hennink*[,†]

[†]Department of Pharmaceutics, Utrecht Institute for Pharmaceutical Sciences (UIPS), Faculty of Science, Utrecht University, 3508 TB Utrecht, The Netherlands
[‡]ChemConnection BV, 5349 AB Oss, The Netherlands
[§]Department of Bio-Organic Chemistry, Eindhoven University of Technology, 5600 MB Eindhoven, The Netherlands
[∥]Department of Clinical Chemistry and Haematology, University Medical Centre Utrecht, 3584 CX Utrecht, The Netherlands
[⊥]Laboratoire de Chimie de Polymères Organiques, Université de Bordeaux, UMR 5629 CNRS, 33607 Pessac, France
[#]Department of Nanomedicine and Theranostics, Institute for Experimental Molecular Imaging RWTH University Clinic, 52074 Aachen, Germany

Supporting Information

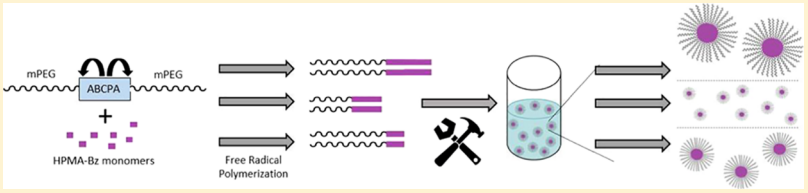

ABSTRACT: Micelles composed of block copolymers of poly(ethylene glycol)-*b*-poly(*N*-2-benzoyloxypropyl methacrylamide) (mPEG-*b*-p(HPMA-Bz)) have shown great promise as drug-delivery carriers due to their excellent stability and high loading capacity. In the present study, parameters influencing micelle size were investigated to tailor sizes in the range of 25−100 nm. Micelles were prepared by a nanoprecipitation method, and their size was modulated by the block copolymer properties such as molecular weight, their hydrophilic-to-hydrophobic ratio, homopolymer content, as well as formulation and processing parameters. It was shown that the micelles have a core−shell structure using a combination of dynamic light scattering and transmission electron microscopy analysis. By varying the degree of polymerization of the hydrophobic block (N_B) between 68 and 10, at a fixed hydrophilic block $mPEG_{5k}$ (N_A = 114), it was shown that the hydrophobic core of the micelle was collapsed following the power law of $(N_B \times N_{agg})^{1/3}$. Further, the calculated brush height was similar for all the micelles examined (10 nm), indicating that crew-cut micelles were made. Both addition of homopolymer and preparation of micelles at lower concentrations or lower rates of addition of the organic solvent to the aqueous phase increased the size of micelles due to partitioning of the hydrophobic homopolymer chains to the core of the micelles and lower nucleation rates, respectively. Furthermore, it was shown that by using different solvents, the size of the micelles substantially changed. The use of acetone, acetonitrile, ethanol, tetrahydrofuran, and dioxane resulted in micelles in the size range of 45−60 nm after removal of the organic solvents. The use of dimethylformamide and dimethylsulfoxide led to markedly larger sizes of 75 and 180 nm, respectively. In conclusion, the results show that by modulating polymer properties and processing conditions, micelles with tailorable sizes can be obtained.

INTRODUCTION

Over the last decades, a large variety of nanomedicines have been developed to improve drug disposition at the target site.[1−5] Particularly, polymeric micelles, core−shell structures composed of amphiphilic polymers, with diameter in the range of 10−100 nm, have attracted much attention. The shell mainly consists of a hydrophilic block, usually poly(ethylene glycol) (PEG), which offers good colloidal stability as well as stealth properties by protecting the micelles from serum/protein interactions and fast uptake by the reticuloendothelial system after injection. The hydrophobic core can accommodate poorly water-soluble drugs like chemotherapeutics for cancer treatment.[6−12]

To have a clinically interesting tumor-targeted nanomedicine, the formulation should provide sufficient stability and drug retention in the blood circulation. This stability can be provided either by physical interactions[13−15] or through

Received: October 23, 2018
Published: November 12, 2018

Scheme 1. Synthesis of mPEG−ABCPA−mPEG Macro-Initiator

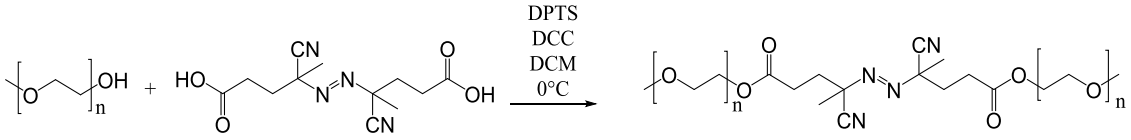

chemical cross-linking.[16] Once circulating in the bloodstream, nanomedicines can penetrate the fenestrated blood capillaries of tumors. Due to the lack of lymphatic drainage, the nanoparticles tend to remain in the tumor region. This phenomenon is the so-called enhanced permeation and retention (EPR) effect.[17−19] Nanomedicines that exploit the EPR effect have shown to both significantly improve therapeutic effects and reduce systemic side effects.[20,21]

It has been shown that the size of nanomedicines, like drug-loaded polymeric micelles, is an important factor for an improved therapeutic efficacy.[22−24] Therefore, in recent years, many studies have been devoted to understanding the effect of size of nanomedicines on their efficacy of cancer treatment. To highlight some of them, Huang et al. demonstrated that tiopronin-coated gold nanoparticles of size 2 and 6 nm have longer blood circulation times and better tumor penetration than 15 nm nanoparticles.[25] Kataoka et al. prepared micelles of different sizes by adding poly(glutamic acid) (p(Glu)) homopolymer to PEG-*b*-p(Glu) copolymer achieving micelle sizes ranging from 30 nm without homopolymer to around 100 nm at a 0.3 homopolymer/copolymer molar ratio. They reported that polymeric micelles in the range of 30−100 nm could penetrate highly permeable tumors, whereas only the micelle formulations that were smaller than 50 nm penetrated poorly permeable tumors and showed antitumor effect.[23] Chilkoti et al. showed that dextrans with a molecular weight of 40−70 kDa did accumulate in tumors after intravenous administration, whereas dextrans of 3.3 and 10 kDa provided deeper and more homogeneous tumor penetration.[26] Shen et al. prepared micelles, based on PEG and a 10-OH methacrylate ester of 7-ethyl-10-hydroxylcamptothecin (PEG-p-(HEMASN38)), of 20−300 nm by varying the process parameters. Although the 100 nm micelles reached a higher concentration at the peripheral side of the tumor compared to the 30 nm size micelles, due to higher liver accumulation of the 30 nm size micelles, this did not translate in an improved therapeutic effect since the latter micelles had better tumor penetration.[22] Smaller nanoparticles also showed better penetration in tumor stroma-containing three-dimensional spheroids, which are a suitable model to study penetration of nanoparticles. The results indicated deeper penetration of 30 nm silica nanoparticles compared to particles of 100 nm.[27] In conclusion, various studies have convincingly demonstrated that smaller drug-loaded particles resulted in better tumor penetration and thus better efficacy of the treatment.[24]

Recently, we have reported on a polymeric micelle formulation based on poly(ethylene glycol)-*block*-poly(*N*-2-benzoyloxypropyl methacrylamide) (mPEG-*b*-p(HPMA-Bz)). Micelles based on this polymer combine excellent particle stability, also in circulation, with improved drug retention as a result of $\pi-\pi$ stacking interactions in the core of the micelles. When loaded with paclitaxel, these micelles have shown very promising results regarding pharmaceutical formulation characteristics (loading and stability) and therapeutic efficacy in animal studies demonstrating complete tumor regression.[28] In the present study, a systematic evaluation was made to understand which parameters affect the size and stability of micelles prepared from mPEG-*b*-p(HPMA-Bz) block copolymers. The goal was to find a robust method to obtain micelles with tailorable sizes in the range of 25−100 nm. This was achieved by synthesizing block copolymers with a hydrophilic 5 kDa poly(ethylene glycol) methyl ether mPEG block; furthermore, some studies were done with a 2 kDa mPEG block copolymer and a varying molecular weight of poly(*N*-2-benzoyloxypropyl methacrylamide) (p(HPMA-Bz)). Furthermore, the effects of formulation variables, including the homopolymer p(HPMA-Bz) content, polymer concentration, and type of solvent, and the effect of processing variables, particularly the rate of addition of the solution of the block copolymer to the aqueous phase, on the size of polymeric micelles were investigated.

MATERIALS AND METHODS

Materials. 4-(Dimethylamino)pyridine (DMAP), *p*-toluenesulfonic acid, 4,4-azobis(4-cyanopentanoic acid) (ABCPA), DL-1-amino-2-propanol, methacryloyl chloride, benzoyl chloride, poly(ethylene glycol) methyl ether (mPEG) 2 kDa, *N*,*N*′-dicyclohexylcarbodiimide (DCC), trichloroacetyl isocyanate (TAIC), bovine serum albumin, and pyrene were obtained from Sigma-Aldrich (Darmstadt, Germany) and used without further purification. mPEG 5 kDa was obtained from Polysciences (Warrington) and dried in a vacuum oven overnight at 70 °C. EasiVial PEG standards for gel permeation chromatography (GPC) analysis were obtained from Agilent (Santa Clara). All solvents were purchased from commercial suppliers and used as received.

Optimized Macro-Initiator (MI) Synthesis. mPEG−ABCPA−mPEG macro-initiators were synthesized through an esterification of mPEG (molecular weight, 2.0 or 5.0 kDa) and ABCPA, using DCC as a coupling reagent and 4-(dimethylamino)pyridinium 4-toluenesulfonate (DPTS, which was made by separately dissolving DMAP and *p*-toluenesulfonic acid in tetrahydrofuran (THF) and mixing the two solutions using a 1:1 molar equivalence) as a catalyst (Scheme 1).[29] ABCPA (1 equiv), mPEG (2 equiv), and DPTS (0.3 equiv) (or 0.280 g of ABCPA, 10 g of mPEG, 0.094 g of DPTS) were dissolved in 50 mL of dry dichloromethane (DCM) and put on ice. Next, 3 equiv of DCC (0.619 g of DCC) were dissolved in 50 mL of DCM and dropwise added to the mPEG solution under nitrogen atmosphere. After addition of DCC, the ice bath was removed allowing the reaction mixture to reach room temperature. After 16 h at room temperature, the reaction mixture was filtered to remove the precipitated 1,3-dicyclohexyl urea and the solvent was removed in vacuo. The product was dissolved in water, stirred for 2 h, and dialyzed against water for 72 h at 4 °C. The sample was freeze-dried to obtain a fluffy white product.

The product was analyzed by GPC using a PSS PFG analytical linear S column and PEGs of narrow molecular weights as calibration standards, as described previously. Samples were prepared by dissolving approximately 5 mg of the MI in 1 mL of dimethylformamide (DMF) containing 10 mM LiCl. Samples of 20 μL were injected, the eluent was DMF containing 10 mM LiCl, the elution rate was 0.7 mL/min, the temperature was 40 °C, and detection was done using a refractive index detector.[30]

The product was further analyzed by ^{1}H NMR spectroscopy (20 mg product was dissolved in 700 μL $CDCl_3$). To determine the unreacted mPEG-OH content, TAIC was added to the sample and analyzed again after 20 min using ^{1}H NMR spectroscopy. After

DOI: 10.1021/acs.langmuir.8b03576
Langmuir 2018, 34, 15495−15506

Scheme 2. Synthesis of mPEG-*b*-p(HPMA-Bz)

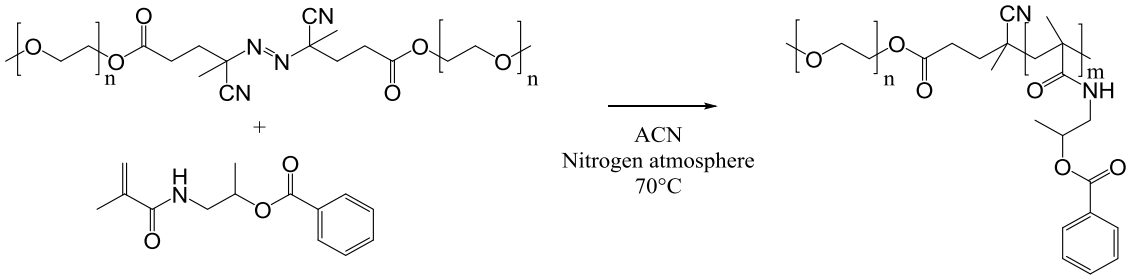

reaction with TAIC, the signal of the methylene group neighboring the terminal hydroxyl group shifts from 4.2 to 4.4 ppm and the amount of unreacted mPEG-OH can subsequently be determined based on the peak areas.[31,32]

Dynamic Light Scattering (DLS). The size of the formed micelles was determined by DLS using a Malvern Zetasizer nano series ZS90 with a measurement angle of 90° and a temperature of 25 °C. Unless stated otherwise, the concentration of the micellar dispersions was 20 mg/mL.

Gas Chromatography Headspace Analysis (GC-Headspace). GC-headspace was conducted to determine the residual solvent contents in the different micellar dispersions using a Shimadzu GC-2010 equipped with a flame ionization detector and a Shimadzu HS-20 headspace autosampler. A 30 m x 0.32 mm capillary column with a film thickness of 0.25 μm was used. An internal standard stock solution was prepared by dissolving 150 μL of 2-propanol (analytical standard) in water in a volumetric 100 mL flask. A small volume (1 mL) of this solution was transferred into a 100 mL volumetric flask and diluted to the 100 mL volume with DMF. Samples were prepared by taking 50 μL of micellar dispersion and dissolving it in 1 mL of DMF, and subsequently, 4 mL of internal standard stock solution was added. The flow rate of nitrogen was 1.8 mL/min. All measurements were done in triplicate.

Cryogenic Transmission Electron Microscopy (Cryo-TEM) Analysis. Cryo-TEM measurements were performed on selected micelles. Samples were prepared on Quantifoil R 2/2 grids. In short, 3 μL of micellar dispersion was pipetted onto the grid and blotted for 3 s using a fully automated vitrification robot (MARK III) at 100% relative humidity. The grid was subsequently plunged and frozen in liquid ethane. Micrographs were taken using an FEI Tecnai G2 Sphere (200 kV electron source) equipped with LaB6 filament utilizing a cryoholder or an FEI Titan (300 kV electron source) equipped with an autoloader station.

Analysis of the Micelles by Asymmetric Flow Field-Flow Fractionation Connected to Multiangle Light Scattering Detector (AF4-MALS). The radius of gyration (R_g) and weight-average molecular weight of some selected micelles (M_w) were determined using a Wyatt DualTec AF4 instrument connected to a Shimadzu LC-2030 Prominence-I system with a Shimadzu LC-2030 autosampler. Fractionation was performed on an AF4 short channel with a 10 kDa membrane of regenerated cellulose and a spacer of 350 μm. The AF4 was connected to a light scattering detector (Wyatt DAWN HELEOS II) installed at 16 different angles ranging from 12.9 to 157.8° using a laser operating at 664.5 nm and a refractive index detector (Wyatt Optilab). Bovine serum albumin dissolved in phosphate-buffered saline (PBS) pH 7.4 with a concentration of 5 mg/mL was used for calibration. The data were analyzed using ASTRA software. Also, to be able to calculate the M_w of micelles using the Zimm plot method,[33] the refraction index increment (dn/dc) of the polymers was measured in water by injection of 600 μL of precisely weighted samples in the range of 6−15 mg/mL and using a flow rate of 0.6 mL/min in an Optilab Rex detector (Wyatt Technology).

Critical Micelle Concentration (CMC) Determination. The CMC of the different block copolymers in water was determined using pyrene as a fluorescent probe.[34,35] Samples were prepared by dissolving the polymers in THF at different concentrations, of which 500 μL was added to 4.5 mL of 120 mM ammonium acetate buffer pH 5.0. This was followed by solvent evaporation. The final polymer concentrations ranged from 1.9×10^{-11} to 1.0 mg/mL. A 15 μL solution of pyrene in acetone (0.18 mM) was added to the polymer solution in buffer, and the solvent was allowed to evaporate overnight. Fluorescence excitation spectra of pyrene between 300 and 360 nm were recorded with an emission wavelength at 390 nm at 37 °C using a UV spectrometer (Jasco FP-8300 Fluorescence Spectrometer). The excitation and emission band slits were 4 and 2 nm, respectively. The intensity ratio I_{338}/I_{333} was plotted against the polymer concentration to calculate the CMC.

Polymer Synthesis. mPEG-*block*-poly(*N*-2-benzoyloxypropyl methacrylamide) (mPEG-*b*-p(HPMA-Bz)) block copolymers were synthesized via free-radical polymerization as described earlier using mPEG−ABCPA−mPEG as a macro-initiator and *N*-(2-benzoyloxypropyl methacrylamide) (HPMA-Bz) as the monomer.[28,34,36] mPEG-*b*-p(HPMA-Bz) block copolymers with different molecular weights of the hydrophobic and hydrophilic block were synthesized either by using $mPEG_{2k}$−ABCPA−$mPEG_{2k}$ or $mPEG_{5k}$−ABCPA−$mPEG_{5k}$ as a macro-initiator or by varying the molar feed ratios of macro-initiator:monomer (1:200, 1:100, 1:75, 1:50, 1:25, 1:12.5 mol/mol) (Scheme 2). In short, the selected macro-initiator and monomer amounts were dissolved at a total concentration of 0.3 g/mL in 20 mL of acetonitrile. The polymerization was conducted at 70 °C in a nitrogen atmosphere for 24 h. The resulting polymers were precipitated in cold diethyl ether and collected after centrifugation. Homopolymers of p(HPMA-Bz) were synthesized and collected in the same way using ABCPA as initiator and HPMA-Bz as monomer. The feed ratios of initiator:monomer were 1:200 (mol/mol), 1:100 (mol/mol), and 1:50 (mol/mol) with a total concentration of 0.3 g/mL in 10 mL of acetonitrile to obtain a total of 2 g of homopolymer after precipitation in cold diethyl ether and centrifugation.

The synthesized polymers were analyzed by ^{1}H NMR spectroscopy. To this end, 20 mg of polymer was dissolved in 700 μL of dimethylsulfoxide (DMSO)-d_6 and the obtained polymer solution was analyzed using a 400 MHz NMR spectrometer with 5 mm PABBO BB probe from Bruker. GPC analysis was conducted to determine the number-average molecular weight (M_n), weight-average molecular weight (M_w), and polydispersity of the synthesized polymers using a PSS PFG analytical linear S column and PEGs of narrow molecular weights as calibration standards. Samples were prepared by dissolving approximately 5 mg of polymer in 1 mL of DMF containing 10 mM LiCl. Samples of 20 μL were injected, the eluent was DMF containing 10 mM LiCl, the elution rate was 0.7 mL/min, the temperature was 40 °C, and detection was done using a refractive index detector.

Micelle Preparation. mPEG-*b*-p(HPMA-Bz) micelles were prepared in triplo by a nanoprecipitation of the polymer dissolved in THF, using water as nonsolvent. First, the polymers were dissolved in THF and the obtained solutions were pipetted into Milli-Q water at a 1:1 volume ratio while stirring. Subsequently, THF was evaporated overnight at room temperature, resulting in the formation of micelles. To investigate the effect of polymer concentration on micellar sizes, the samples were prepared using 5, 10, 20, 30, and 40 mg/mL of polymer solution. Additionally, an experiment was carried out where the volume ratio of solvent to water was decreased from 1:1 to 0.6:1 and 0.3:1. Addition of the polymer/solvent solution to water

DOI: 10.1021/acs.langmuir.8b03576
Langmuir 2018, 34, 15495−15506

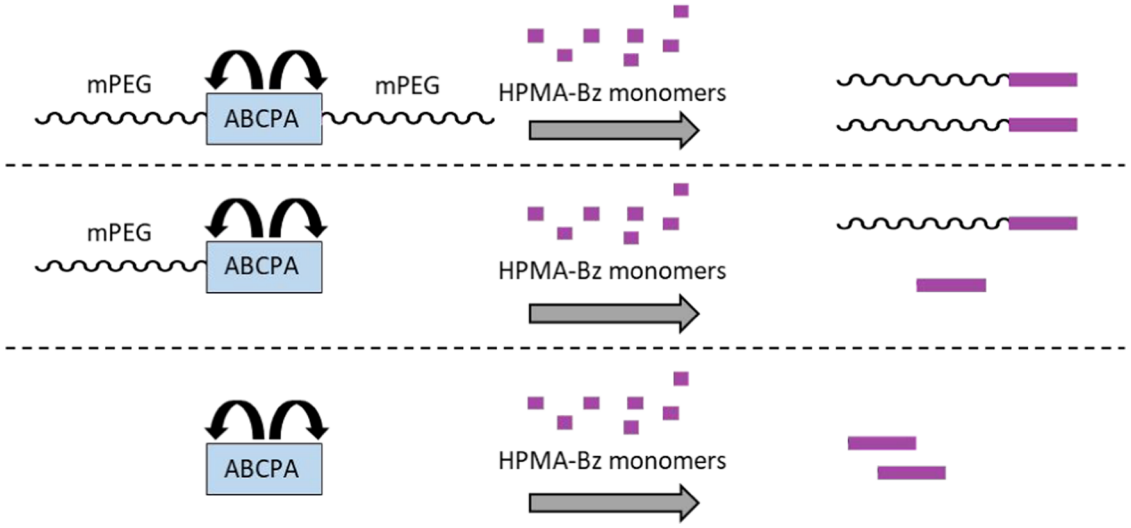

Figure 1. Schematic representation of the polymerization of mPEG-*b*-p(HPMA-Bz) initiated by mPEG−ABCPA−mPEG results in the synthesis of mPEG-*b*-p(HPMA-Bz) diblock copolymers only. Initiation by mPEG−ABCPA will result in a mixture of block copolymer and homopolymer p(HPMA-Bz). Initiation by ABCPA will result in the formation of homopolymer only. It is hereby assumed that no chain transfer occurs.

was performed rapidly using a pipette while stirring. The final polymer concentrations in water were 10, 20, and 30 mg/mL. Thus, in total, nine different conditions were tested. In the remainder of the experiments, the polymer concentration was fixed at 20 mg/mL, unless mentioned otherwise. Besides THF, the following solvents were also used: acetonitrile, acetone, 1,4-dioxane, dimethylformamide (DMF), dimethylsulfoxide (DMSO), and ethanol. For the less/nonvolatile solvents (dioxane, DMSO, DMF, and ethanol), the residual solvent was removed by dialysis using a Spectra/Por dialysis membrane with a molecular weight cutoff of 6−8 kDa. Moreover, the aqueous phase was varied: water, 0.9% NaCl solution, PBS (containing 3.1 g of Na_2HPO_4, 0.3 g of NaH_2PO_4, and 8.2 g of NaCl in 1 L pH 7.4), and 120 mM ammonium acetate buffer pH 5.0 were used. The addition rates were varied by introducing the polymer solution in THF into the aqueous phase using a peristaltic pump (Pharmacia LKB pump P-1, made in Sweden) at 0.15 and 1.5 mL/min while stirring using a magnetic stirrer. Also, the effect of adding Milli-Q water to the polymer solution in THF in a 1:1 volume ratio was investigated.

Effect of the Presence of p(HPMA-Bz) Homopolymer and the Presence of Free mPEG on the Size of Polymeric Micelles. Samples of 20 mg of mPEG-*b*-p(HPMA-Bz) and 0, 1, 2, 5, and 10 mg of p(HPMA-Bz) were dissolved in 1 mL of THF corresponding to weight fractions of 0, 5, 9, 20, and 33 wt % of the homopolymer. Other samples of 20 mg of mPEG-*b*-p(HPMA-Bz) and 0, 1, 2, 5, and 10 mg of $mPEG_{5k}$ were dissolved in 1 mL of THF corresponding to weight fractions of 0, 5, 9, 20, and 33 wt % of the $mPEG_{5k}$. Addition of the polymer solution to water was performed rapidly using a pipette while stirring. THF was evaporated overnight at room temperature, resulting in the formation of micelles.

RESULTS AND DISCUSSION

mPEG−ABCPA−mPEG Macro-Initiator Synthesis. The macro-initiator (MI) used for polymerization, mPEG−ABCPA−mPEG, was previously synthesized by the reaction of 2 equiv mPEG with 1 equiv 4,4-azobis(4-cyanopentanoic acid) (ABCPA).[31,37] According to this previous procedure, all of the components except mPEG were dissolved simultaneously in a 1:1 mixture of DCM and dry DMF and put on ice. In this way, the COOH groups of ABCPA were first activated with DCC and subsequently mPEG was added. After addition of mPEG, the ice bath was removed, and the mixture was stirred at room temperature overnight. This resulted in a yield of ∼80% of macro-initiator after precipitation.[37] This strategy, however, led to a large amount of ∼40% byproduct with a molecular weight of 5 kDa according to GPC analysis (see Supporting Information (SI)). The shoulder peak in GPC can be due to the presence of either mPEG−ABCPA or unreacted mPEG, or a combination of both. It is known that a DCC-activated ester can undergo a rearrangement reaction to yield an *N*-acyl iso-urea product, which is not reactive with the primary hydroxyl group of mPEG.[38] Therefore, there is a possibility that the ABCPA reacts with only one mPEG chain giving mPEG−ABCPA, with or without acyl urea (see SI), as a byproduct. Consequently, unreacted mPEG-OH (free mPEG) will also be present in the reaction solution. TAIC is a reagent that is used for the quantitative determination of hydroxy end-groups of polymers using ^{1}H NMR spectroscopy.[32,39] Therefore, this reagent was used to quantify the amount of free mPEG in the obtained product. Analysis showed the presence of ∼30% unreacted mPEG, leaving the remaining 10% of the 5 kDa byproduct to be mPEG−ABCPA. Further purification steps such as dialysis could not separate the byproducts from mPEG−ABCPA−mPEG.

Upon the use of MI contaminated with mPEG−ABCPA for the polymerization of HMPA−Bz, both the p(HPMA-Bz) homopolymer and the aimed mPEG-*b*-p(HPMA-Bz) block copolymer are formed (Figure 1). The presence of the p(HPMA-Bz) is unwanted because it will be solubilized in the core of the micelles, which, in turn, will result in an increase in micellar size. Therefore, the MI synthesis was optimized to obtain a high yield of mPEG−ABCPA−mPEG and to minimize the amounts of the mPEG−ABCPA−mPEG byproducts.

In the new procedure, all reagents, including mPEG but except DCC, were dissolved in DCM. Subsequently DCC dissolved in DCM was added dropwise.[29] This resulted in activation of the COOH groups in the presence of mPEG to allow reaction of its OH group with the active ester, thereby reducing the possibility for the formation of the inactive *N*-acyl iso-urea product. Furthermore, contrary to the other procedure, no DMF was used and the reaction was therefore conducted in the less polar solvent DCM.

DOI: 10.1021/acs.langmuir.8b03576
Langmuir 2018, 34, 15495−15506

Table 1. Characteristics of the Synthesized mPEG-*b*-p(HPMA-Bz) Block Copolymers as Determined by ^{1}H NMR and GPC Analyses

polymer	MI/M	M_n by ^{1}H NMR (kDa)	M_n by GPC (kDa)	M_w by GPC (kDa)	polydispersity (M_w/M_n) (GPC)	yield (%)
$mPEG_{5k}$-*b*-p(HPMA-Bz)$_{18.5k}$	1:200	23.5	18.9	21.1	1.12	72
$mPEG_{5k}$-*b*-p(HPMA-Bz)$_{9.6k}$	1:100	14.6	17.3	19.6	1.13	79
$mPEG_{5k}$-*b*-p(HPMA-Bz)$_{7.7k}$	1:75	12.7	16.4	18.7	1.14	81
$mPEG_{5k}$-*b*-p(HPMA-Bz)$_{4.7k}$	1:50	9.7	15.1	17.4	1.15	83
$mPEG_{5k}$-*b*-p(HPMA-Bz)$_{2.2k}$	1:25	7.2	12.8	14.8	1.16	83
$mPEG_{5k}$-*b*-p(HPMA-Bz)$_{1.0k}$	1:12.5	6.0	9.8	12.2	1.23	84
$mPEG_{2k}$-*b*-p(HPMA-Bz)$_{20.6k}$	1:200	22.6	13.5	19	1.42	59
$mPEG_{2k}$-*b*-p(HPMA-Bz)$_{10.9k}$	1:100	12.9	10.7	16	1.51	74
$mPEG_{2k}$-*b*-p(HPMA-Bz)$_{7.7k}$	1:75	9.7	8.5	17.1	1.57	53
$mPEG_{2k}$-*b*-p(HPMA-Bz)$_{5.3k}$	1:50	7.3	8.1	12.6	1.55	87
$mPEG_{2k}$-*b*-p(HPMA-Bz)$_{2.6k}$	1:25	4.6	5.7	8.2	1.45	82
$mPEG_{2k}$-*b*-p(HPMA-Bz)$_{1.2k}$	1:12.5	3.2	4.4	5.7	1.31	87

The new procedure resulted in the successful synthesis of two different mPEG−ABCPA−mPEG macro-initiators ($mPEG_{5k}$ and $mPEG_{2k}$), which were obtained in a yield of ∼90% and only contained ∼5% of the mixture of 5 kDa mPEG−ABCPA/free mPEG (GPC analysis, Figure S1). The amount of free mPEG was determined by ^{1}H NMR spectroscopy using TAIC to be 4.2% (Figure S2). This shows that the MI only contained a trace amount of 0.8% mPEG−ABCPA. Therefore, the MI synthesized according to this new procedure was used for the synthesis of different mPEG-*b*-p(HPMA-Bz) block copolymers.

Synthesis of mPEG-*b*-p(HPMA-Bz) Block Copolymers. Amphiphilic mPEG-*b*-p(HPMA-Bz) block copolymers with varying molecular weights of the hydrophobic and hydrophilic blocks were synthesized by free-radical polymerization of HPMA-Bz using mPEG−ABCPA−mPEG macro-initiators ($mPEG_{5k}$ or $mPEG_{2k}$) (Figure 1) at different macro-initiator/monomer ratios (MI/M; Table 1). The molecular weights (M_n, M_w) of the obtained polymers were determined by ^{1}H NMR and GPC analyses. As reported earlier, an increasing trend of molecular weight was observed upon increasing the monomer-to-initiator ratio.[34]

The average kinetic chain length for free-radical chain polymerization is defined as the average number of monomers polymerized per initiated chain and is proportional to the monomer concentration $[M_0]$ divided by the square root of the initiator concentration $[I_0]^{-1/2}$.[40,41] Plotting the number-average molecular weight (M_n) as measured by ^{1}H NMR spectroscopy analysis against the average kinetic chain length indeed resulted in a linear correlation for both the $mPEG_{5k}$ and $mPEG_{2k}$ block copolymers (Figure 2) as also observed previously by us for the block copolymer mPEG-*b*-pHPMAmLac$_n$ (methoxy poly(ethylene glycol)-*b*-poly[*N*-(2-hydroxypropyl) methacrylamide-lactate]).[30]

Residual Solvent and Kinetics of Micelle Formation. To get insight into the kinetics of micelle formation and the rate of removal of THF, in which the $mPEG_{5k}$-*b*-p(HPMA-Bz)$_{18.5k}$ polymer was dissolved at 20 mg/mL, the size of micelles was followed in time after direct addition of the THF/polymer solution to water (THF/water was 1:1 v/v). The hydrodynamic diameters of the micelles were measured using DLS, and the THF content was measured using GC-headspace analysis directly after addition (0 h) and at regular time intervals up to 96 h (Figure 3). Directly after addition of the polymer solution to water, particles with a hydrodynamic diameter of approximately 80 nm and a polydispersity index of

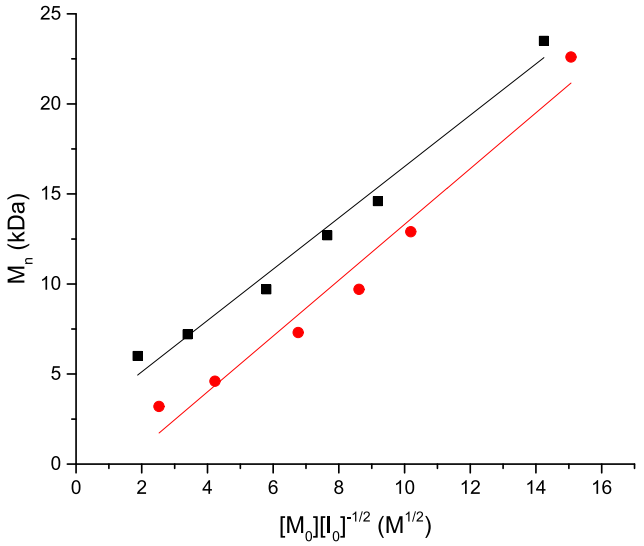

Figure 2. Linear correlation between the number-average molecular weight (M_n) as measured by ^{1}H NMR spectra of mPEG-*b*-p(HPMA-Bz) as a function of the feed molar concentration of monomer divided by the square root of the feed molar concentration of initiator ($[M_0][I_0]^{-1/2}$) (black: $mPEG_{5k}$-*b*-p(HPMA-Bz)$_n$ with r^2 = 0.98; red: $mPEG_{2k}$-*b*-p(HPMA-Bz)$_n$ with r^2 = 0.97).

less than 0.1 were formed. After 24 h, the micelles showed a decrease in size to 50 nm, and a residual THF content of ∼3000 ppm was detected. At 25 h, the micellar dispersion was spiked with an additional 50 volume percentage of THF, which resulted in an immediate increase in micelle size from 50 to 70 nm. It can therefore be concluded that there is a direct correlation between the remaining amount of THF and the hydrodynamic diameter of the micelles. It should be noted that the final micelle size of 50 nm was already reached at THF concentrations of less than 10^5 ppm. Addition of THF to the micellar dispersion showed that the core of the micelles can become swollen by accommodating part of the added THF. After 48 h of evaporation, the residual THF content was ∼3000 ppm, which is not sufficient to obtain a product within the acceptable range below 720 ppm according to the International Council of Harmonization of Technical Requirements for Registration of Pharmaceuticals for Human Use.[42] Therefore, the evaporation time was extended to 96 h and the micellar dispersion was also dialyzed against water to remove any residual THF. The final THF content after dialysis and

DOI: 10.1021/acs.langmuir.8b03576
Langmuir 2018, 34, 15495−15506

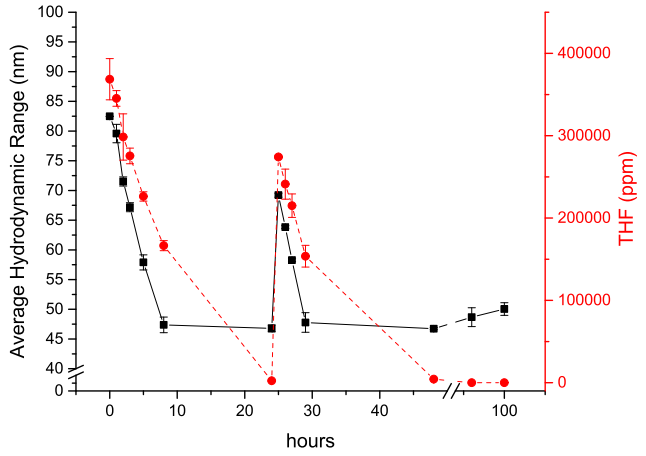

Figure 3. Average hydrodynamic diameters (black) of mPEG$_{5k}$-*b*-p(HPMA-Bz)$_{18.5k}$ micelles and THF concentration (red) of the micellar dispersion as a function of time. At 25 h, the dispersion was spiked with THF. After a second overnight evaporation (48 h) and subsequent over weekend evaporation (96 h), the samples were dialyzed overnight, which is represented at time point 100 h in the graph.

measured by GC-headspace was below the detection limit (10 ppm).

Effect of the Hydrophobic/Hydrophilic Block Molecular Weight of mPEG-*b*-p(HPMA-Bz) on the Micelle Size. To investigate the effect of the hydrophobic/hydrophilic block molecular weight of the polymers on the micelle size, micelles were prepared from the synthesized polymers of Table 1. The polymers were dissolved in THF at 20 mg/mL and used to prepare micelles through the nanoprecipitation method in water, as described in the Materials and Methods section. All mPEG$_{5k}$ block copolymers formed micelles as was demonstrated by cryo-TEM and DLS analyses.

Both the DLS and the cryo-TEM results showed that the micelle size proportionally increased from the smallest to largest molecular weights of the hydrophobic block from 30 to 48 nm for the hydrodynamic diameter and from 9 to 28 nm for the cryo-TEM diameter (Figures 4 and S4). The DLS polydispersities were lower than 0.1 pointing to a narrow size distribution, which is in agreement with the results of the TEM pictures. More precisely, the histograms of the TEM diameters based on ∼100 to ∼400 micelles (for mPEG$_{5k}$-*b*-p(HPMA-Bz)$_{18.5k}$ and mPEG$_{5k}$-*b*-p(HPMA-Bz)$_{2.2k}$ copolymers, respectively) exhibited normalized standard deviations of 25% at most (.). The hydrated layer of the micelles was estimated by the difference of radii between the radius of hydration (R_h) and the radius as determined by TEM (R_{TEM}) and appeared to be constant for the four samples (approximately 10 nm; Table 2).

The radius of gyration (R_g), radius of hydration (R_h), and M_w of the micelles based on a selection of mPEG$_{5k}$ polymers of Table 1 were determined by AF4-MALS (Table 2). The ratio of R_g/R_h is structure-sensitive and provides information about the morphology of a system. The ratio for rigid spherical structures with a uniform density is $\sqrt{3/5} \approx 0.775$.[43−45] Structures with a dense core and a partly coiled less dense shell (core−shell structures) show a smaller R_g and therefore have R_g/R_h values lower than 0.775.[43−48] Based on the MALS data, the produced mPEG$_{5k}$-*b*-p(HPMA-Bz) micelles had a core−shell structure because the R_g/R_h ratios were between 0.59 and

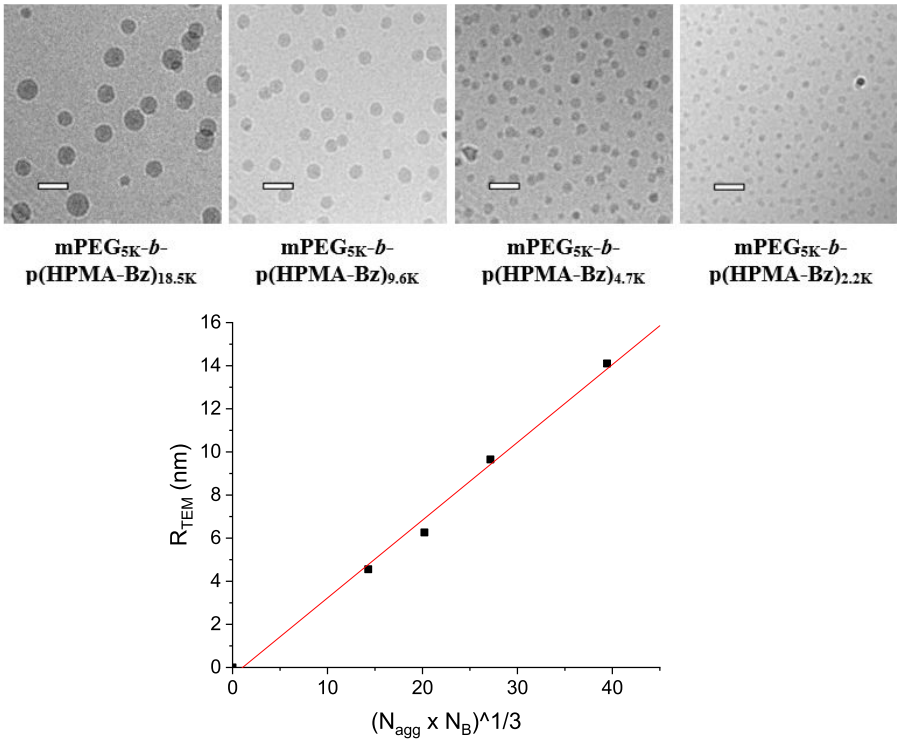

Figure 4. (Top) Cryo-TEM images showing particle size variation upon molecular weight changes of the mPEG$_{5k}$ block copolymers used; the scale bars correspond to 50 nm. (Bottom) Average micelle core diameter measured by cryo-TEM as a function of the cubic root of the product of the degree of polymerization (N_B) of the hydrophobic blocks of the copolymers as determined by ^{1}H NMR spectroscopy, and the aggregation number (N_{agg}) of the corresponding micelles revealed by AF4-MALS, r^2 = 0.99.

DOI: 10.1021/acs.langmuir.8b03576
Langmuir 2018, 34, 15495−15506

Table 2. Characteristics of $mPEG_{5k}$-*b*-p(HPMA-Bz) Micelles Prepared from a 20 mg/mL THF Solution and Determined by AF4-MALS[a]

polymer	R_g (nm)	R_h (nm)	R_{TEM} (nm)	R_g/R_h	$M_{w(mic)}$ (10^6 Da)	N_{agg}	$\sigma^{-1} = d^2$ (nm^2)	H (nm)	$R_h - R_{TEM}$ (nm)
$mPEG_{5k}$-*b*-p(HPMA-Bz)$_{18.5k}$	15	24	14.1	0.63	21.2	905	8.2	8.9	9.9
$mPEG_{5k}$-*b*-p(HPMA-Bz)$_{9.6k}$	12	20	9.6	0.59	7.5	513	9.3	8.4	10.4
$mPEG_{5k}$-*b*-p(HPMA-Bz)$_{4.7k}$	12	18	6.3	0.63	4.0	416	10.0	8.3	11.7
$mPEG_{5k}$-*b*-p(HPMA-Bz)$_{2.2k}$	10	15	4.6	0.64	2.1	291	10.0	8.4	10.4

[a] R_g = Radius of gyration; R_h = hydrodynamic radius; R_{TEM} = radius as measured by TEM; $M_{w(mic)}$ = weight-average molecular weight of the micelles; N_{agg} = the micelle aggregation number; σ^{-1} = mean surface area per molecule calculated by $\sigma^{-1} = d^2 = 4\pi R_h^2/N_{agg}$, where d is the interchain distance; H = shell brush height calculated by the de Gennes–Alexander model $H = N_A a_A (a_A/d)^{2/3}$.

0.64 and thus lower than that of typical rigid spheres. This core–corona structure was also confirmed using ^{1}H NMR analysis of the micelles dispersed in deuterium oxide (D_2O) (shown in Figure S6). The ^{1}H NMR spectrum of mPEG-*b*-p(HPMA-Bz) block copolymer dissolved in DMSO-d_6 (Figure S6) showed resonances that can be assigned to the protons of both mPEG as the hydrophilic part (3.40–3.60 ppm) and p(HPMA-Bz) as the hydrophobic block (5.25 ppm and 7.25–8.25 ppm). The self-assembled structure of the mPEG-*b*-p(HPMA-Bz) block copolymer in D_2O only showed resonances belonging to the mPEG block of the copolymer, whereas the peaks of the p(HPMA-Bz) block completely disappeared due to suppression of molecular motion of the hydrophobic part inside the core of the micelles.[49,50]

AF4-MALS also revealed that the micelle aggregation number (N_{agg}), calculated by dividing the weight-average molecular weight of the micelles ($M_{w(mic)}$) by the M_n of the polymer as determined by ^{1}H NMR analysis, decreased with decreasing molecular weight of the hydrophobic block of the block copolymer. This was also observed in dissipative particle dynamic simulations of A–B diblock copolymers by Li et al. and Sheng et al., where N_{agg} increases by either increasing the hydrophobic interaction energy through varying the repulsive parameter within the hydrophobic block B or decreasing the molecular weight of the hydrophilic block A.[51,52] In our system, the molecular weight of the hydrophobic block B was varied between 2.2 and 18.5 kDa, which corresponds to degrees of polymerization N_B between 10 and 68, whereas the molecular weight of the hydrophilic block A was kept at 5 kDa (N_A = 114). However, even the lowest M_n of the hydrophobic block p(HPMA-Bz) of 2.2 kDa still provided sufficient hydrophobicity for micelle formation by creating a packed core structure. Already indicated by the disappearance of the B block peaks in ^{1}H NMR spectroscopy, this statement can also be proved by a polymer physics consideration. As shown in Figure 4, the TEM radii that reflect the hydrophobic cores of the micelles follow a power law with the product of N_B and N_{agg} of exponent 1/3, characteristic for a collapsed state of the B block chains.[53] On the opposite, the mPEG chains of the corona are highly swollen by water, making them invisible on the TEM images. The surface area per mPEG chain was calculated by dividing the surface area of the micelles ($4\pi R_h^2$) by the number of molecules (N_{agg}) and assimilated with the square of the interchain distance (d), neglecting a geometrical prefactor. This spacing between mPEG molecules remained approximately the same for all samples ($d \sim 3.0 \pm 0.1$ nm) since both N_{agg} and the hydrated radius (R_h) decreased simultaneously when N_B was decreased. When using the de Gennes–Alexander theory of polymer brushes, the mPEG height was estimated by $H = N_A a_A (a_A/d)^{2/3}$.[54−56] The values obtained by this model are shown in Table 2 and were found approximately constant $H \sim 8.5 \pm 0.3$ nm, using N_A = 114 and a Kuhn length per mPEG segment a_A = 0.33 nm obtained from the bond lengths and coarse grain simulations.[57] In agreement with the constant difference of ~10 nm that was observed between R_h and R_{TEM}, one can deduce that the mPEG chains forming the corona of the micelles are densely packed and in a stretched conformation (brush regime). However, there was no curvature effect on the brush height as there was no variation observed with the micelle core size, which corresponds to the "crew-cut" regime of micelles rather than the "starlike" regime that would require longer hydrophilic blocks.[58] Of the $mPEG_{2k}$ copolymers, only $mPEG_{2k}$-*b*-p(HPMA-Bz)$_{2.6k}$ and $mPEG_{2k}$-*b*-p(HPMA-Bz)$_{1.2k}$ formed clear micellar dispersions with a size of the micelles of 25 nm and polydispersity lower than 0.2. On the other hand, the block copolymers with higher molecular weight of the hydrophobic block (between 5.3 and 20.6 kDa; see Table 1) aggregated after THF evaporation. Cryo-TEM analysis of $mPEG_{2k}$-*b*-p(HPMA-Bz)$_{20.6k}$ after nanoprecipitation confirmed that mainly aggregates were formed, yet showing an interesting internal structure appearing as densely packed spherical globules (Figure S9). Typically, the spherical micelle shape is stable if the core diameter does not exceed too much the dimensions of the corona, which is estimated at 3.3 nm using the de Gennes–Alexander formula with N_A = 45 for $mPEG_{2k}$. This is the case when the right balance of hydrophilic-to-hydrophobic ratio is used. When increasing the hydrophobic content, this will eventually cause phase separation, as mentioned by Sheng et al.[52] In other words, the ratio between the hydrophilic and hydrophobic block influences the critical packing parameter, which in turn can predict whether either micelles or aggregates are formed. These scaling laws state that once the effective hydrophilic surface area at the aggregate solution interface is reached, the volume occupied by the hydrophobic chains in the aggregate core becomes too large to be able to form spherical vesicles.[59,60] Cylindrical and lamellar aggregates, as well as aggregated precipitated structures will, in these cases, be observed as is the case for the $mPEG_{2k}$ block copolymers with higher molecular weight of the hydrophobic block.

Critical Micelle Concentration Determination. The critical micelle concentrations (CMCs) of the polymers of Table 1 were determined using the commonly used pyrene method. Pyrene is a hydrophobic fluorescent molecule that shows a shift of the excitation wavelength (from 300 to 360 nm) as a result of its partitioning in the hydrophobic core of polymeric micelles.[35] Figure 5 shows the CMC values for the block copolymers with a fixed hydrophilic mPEG block of 5 kDa and a varying molecular weight of the hydrophobic p(HPMA-Bz) block. For the polymer $mPEG_{5k}$-*b*-p(HPMA-Bz)$_{18.5k}$ (total M_w of 23.5 kDa), the CMC is 2.3 μg/mL. On

DOI: 10.1021/acs.langmuir.8b03576
Langmuir 2018, 34, 15495−15506

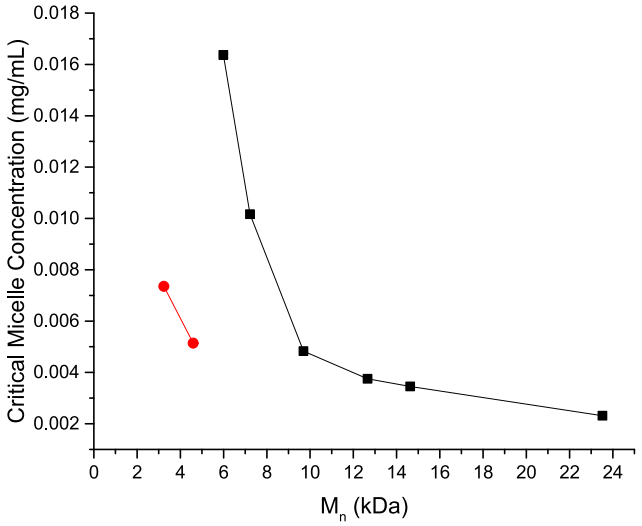

Figure 5. Critical micelle concentration as a function of polymer molecular weight. The black line shows the CMC of the polymers with a fixed mPEG of 5 kDa, whereas the red line shows the CMC of the polymers with a fixed mPEG of 2 kDa.

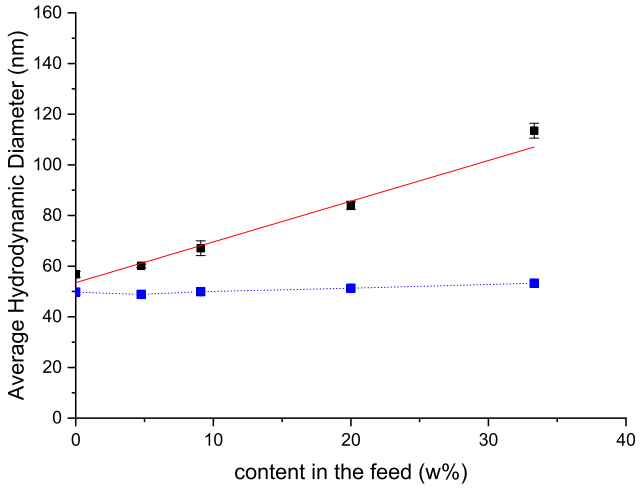

Figure 6. Average hydrodynamic diameter of $mPEG_{5k}$-*b*-$p(HPMA\text{-}Bz)_{18.5k}$ in black/red as a function of homopolymer content in the feed, and in blue as a function of free $mPEG_{5k}$ content in the feed (n = 3).

the other hand, the block copolymer with the smallest hydrophobic block $mPEG_{5k}$-*b*-$p(HPMA\text{-}Bz)_{1.0k}$ (total M_w of 6 kDa) had a CMC of 16.4 μg/mL. This demonstrates that a block copolymer with only about five monomeric units in the hydrophobic block is already able to form micelles pointing to strong $\pi-\pi$ stacking interactions. It was also shown that the CMCs of the polymers decreased with increasing molecular weight of the hydrophobic block. This trend has previously been reported in the literature.[50,61,62] The CMCs of $mPEG_{2k}$-*b*-$p(HPMA\text{-}Bz)_{2.6k}$ and $mPEG_{2k}$-*b*-$p(HPMA\text{-}Bz)_{1.2k}$ are 5.1 and 7.4 μg/mL, respectively (Figure 5). These CMCs are still lower compared to those of $mPEG_{5k}$-*b*-$p(HPMA\text{-}Bz)_{2.2k}$ and $mPEG_{5k}$-*b*-$p(HPMA\text{-}Bz)_{1.0k}$, with values of 10.2 and 16.4 μg/mL, respectively, where the only difference between those polymers is the molecular weight of the hydrophilic mPEG block being 2 or 5 kDa. Therefore, as expected and previously shown for other systems, it can be concluded that both the size of the hydrophobic block and the hydrophilic/hydrophobic ratio determine the CMC value.[63,64]

Effect of Free Homopolymer and Free PEG on the Size of Micelles. To investigate the effect of homopolymer in the polymer mixture on micelle size, homopolymers p(HPMA-Bz) were synthesized with M_n values of 14.5, 11.2, and 5.5 kDa. Subsequently, known amounts of the $p(HPMA\text{-}Bz)_{14.5k}$ homopolymer together with $mPEG_{5k}$-*b*-$p(HPMA\text{-}Bz)_{18.5k}$ were dissolved in THF and added to water to obtain micelles with polydispersities lower than 0.2. Figure 6 shows that with increasing amounts of homopolymer in the THF solution, the size of the obtained micelles increased proportionally. Since the $p(HPMA\text{-}Bz)_{14.5k}$ homopolymer is very hydrophobic, it will very likely partition inside the hydrophobic core of the micelles, resulting in an increase in micellar size. Similar results were observed for $mPEG_{5k}$-*b*-$p(HPMA\text{-}Bz)_{9.6k}$ and $mPEG_{5k}$-*b*-$p(HPMA\text{-}Bz)_{4.7k}$, upon addition of homopolymers with M_n of 11.3 and 5.5 kDa to the feed, respectively (Figure S10). Figure S10 shows that the effect of the added homopolymer on the size of the micelles is larger for micelles made of polymers with a smaller hydrophobic domain. A possible explanation is that block copolymers with a smaller hydrophobic block are relatively more soluble in water, as also shown by a higher CMC, making them more susceptible to the conditions at which the mixing and solvent shifting occur. Additionally, the N_{agg} of the micelles is lower for the smaller polymers. Therefore, incorporation of homopolymer in the core of the micelles based on lower polymer molecular weight increases the size of micelle more drastically.

Figure 6 and previous studies of Kataoka et al.[23] and Kimura et al.[65] show that the presence of homopolymer in the feed can be exploited to tailor the size of polymer micelles. Kataoka et al. mixed poly(glutamic acid) homopolymer with PEG-*b*-poly(glutamic acid) to control the size of micelles,[23] and Kimura et al. used poly(L-lactic acid) homopolymer to control the size of (sarcosine)-*b*-(L-lactic acid) nanoparticles.[65]

Besides p(HPMA-Bz), the block copolymer mixture might also contain less than 5% free mPEG (see SI). We therefore also examined the effect of free mPEG on the size of micelles by adding excess amounts of mPEG to the polymer mixture (Figure 6). The presence of up to 40% of free mPEG did not result in changes in micelle size, which is probably due to the high solubility of $mPEG_{5k}$ in water.

Effect of Polymer Concentration and Rate of Addition on Micelle Size. Micelles were prepared by addition of THF with varying concentrations of $mPEG_{5k}$-*b*-$p(HPMA\text{-}Bz)_{18.5k}$ block copolymers. Figure 7 shows that the hydrodynamic diameter of the formed micelles decreased from approximately 80 to 50 nm with increasing polymer concentration in THF. Concomitantly, the micelles had a smaller size distribution at higher initial polymer concentrations, as indicated by the decreasing indices from 0.3 to less than 0.1. Similar results were observed for $mPEG_{5k}$-*b*-$p(HPMA\text{-}Bz)_{9.6k}$ and $mPEG_{5k}$-*b*-$p(HPMA\text{-}Bz)_{4.7k}$ from approximately 50 to 42 nm and from approximately 42 to 36 nm, respectively, upon increasing the polymer concentration in THF (Figure S10). These results suggest that the self-assembly is based on a nucleation-controlled process, where the size of micelles is dependent on the nucleation rate. A larger number of nuclei will thereby result in smaller micelles.[66] This trend was also observed in the study of Caron et al., where higher initial concentration of squalenoyl prodrug in the organic phase yielded smaller self-assemblies.[67] The dependence of concentration on the resulting micelle size was also confirmed

DOI: 10.1021/acs.langmuir.8b03576
Langmuir 2018, 34, 15495−15506

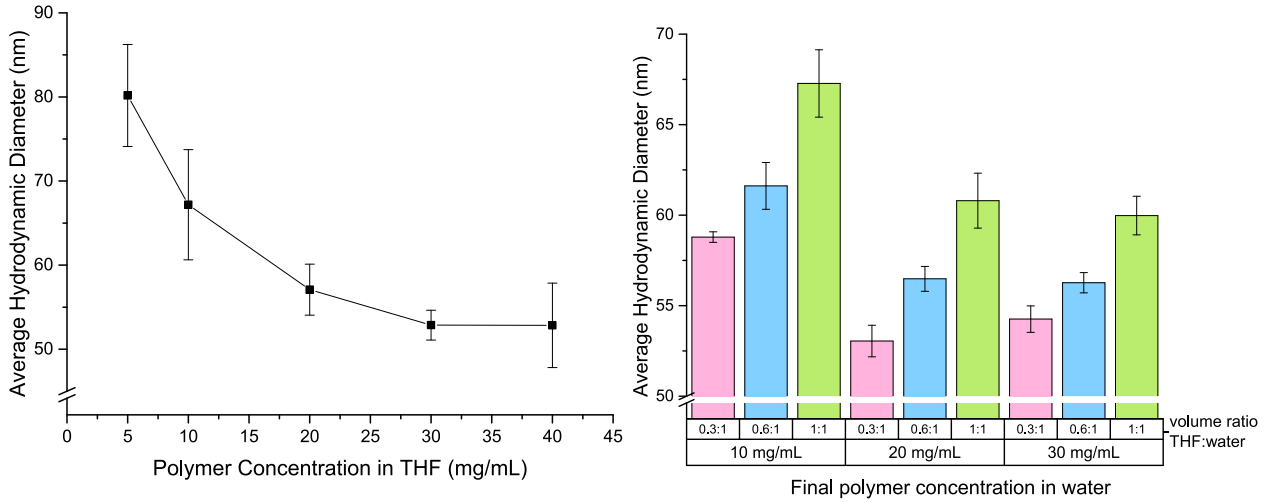

Figure 7. (Left) Hydrodynamic diameters of micelles as a function of the polymer concentration in THF added to water in a 1:1 ratio. (Right) Effect of changing the concentration of polymer in THF using different THF-to-water volume ratios. The final polymer concentrations were 10, 20, and 30 mg/mL (n = 3).

in another experiment where the final concentration of the polymer in the water phase after THF evaporation was fixed at 10, 20, and 30 mg/mL, but the ratio of organic solvent to water was reduced from 1:1 to 0.3:1 using less THF (0.3, 0.6, and 1 mL) to dissolve the same amount of polymer (Figure 7). Higher initial polymer concentrations in the organic phase upon mixing with the water phase led to higher supersaturation and consequently to more nuclei and smaller micelles. Also, at higher THF content, the supersaturation state is lower, decreasing nucleus formation. Therefore, as expected, smaller micelles were obtained at 0.3:1 compared to 1:1 volume ratio.[68] Furthermore, the size of the micelles reached a minimum at approximately 50−55 nm, suggesting that a critical particle size was obtained and increasing the concentration did not affect the size anymore.[69]

As the nucleation rate is dependent on supersaturation and is also affected by the quality of mixing, different rates of addition of organic polymer solution to aqueous phase were used to manipulate the supersaturation state. Thus, micelles were prepared at different addition rates of the polymer solution to water and by fast addition of water to the organic phase (Figure 8). The hydrodynamic diameters of mPEG5K-*b*-p(HPMA-Bz)$_{18.5k}$ micelles after THF evaporation were 82 and 62 nm with polydispersities of less than 0.1 and 0.2 at addition rates of 0.15 and 1.5 mL/min, respectively. Also, the sizes of the micelles upon rapid addition of the polymer solution to the water phase and the water phase to the polymer solution were 58 and 56 nm, respectively, with polydispersities of less than 0.1, reaching the minimal micelle size. This is similar to the finding reported by Aliabadi et al., in which no significant difference in size of MePEO-*b*-PCL micelles prepared by addition of water to acetone or acetone to water was observed.[70] As expected, similar results were observed using mPEG$_{5k}$-*b*-p(HPMA-Bz)$_{9.6k}$ and mPEG$_{5k}$-*b*-p(HPMA-Bz)$_{4.7k}$ polymers (Figure S12). However, the polydispersities of the micellar dispersions were higher (0.35 and 0.45) at 0.15 mL/min rate of addition (Figure S12). Generally, during nanoprecipitation, both nucleation and particle growth occur in the water/THF mixture even before complete mixing. So, when the polymer solution is added slowly to water, there is a continuous change in the composition of the mixture, which

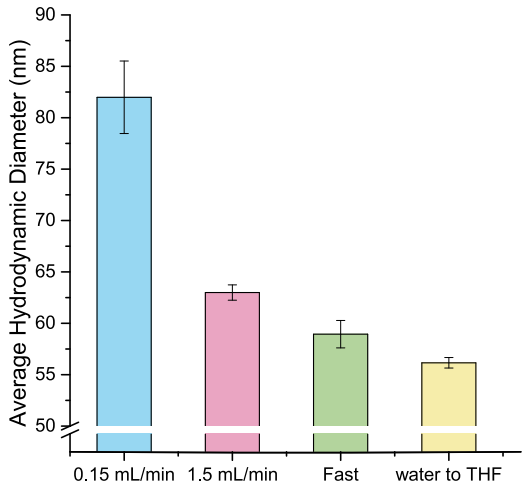

Figure 8. Effect of rate of addition of the polymer solution in THF to the aqueous phase on micelle size; the samples were stirred during and until 1 min after addition of the polymer solution to aqueous buffer (n = 3).

results in less homogeneous supersaturation. Fast addition of THF to water, on the other hand, results in a fast mixing, which, in turn, is associated with rapid supersaturation causing the formation of smaller nuclei and thus smaller and more monodisperse micelles.[71]

Effect of Different Solvents and Buffers on Micelle Size. The effect of the type of organic solvent on the size of HPMA-Bz micelles was also investigated. THF, acetonitrile, acetone, ethanol, 1,4-dioxane, DMSO, and DMF were used because of their miscibility with water and ability to dissolve the mPEG-*b*-p(HPMA-Bz) block copolymers. The polymer concentrations in organic solvent were fixed at 20 mg/mL to avoid the effect of polymer concentration on the nanoprecipitation process. In the case of ethanol, the polymer was only soluble at temperatures above ∼60 °C and thus the micelle preparation was conducted using polymer solutions and water at 70 °C. Subsequently, the solvents were removed by either evaporation (for THF, acetonitrile, and acetone) or, in the case of less volatile solvents like dioxane, DMSO, DMF, and ethanol, by dialysis. As depicted in Figure 9, the use of

DOI: 10.1021/acs.langmuir.8b03576
Langmuir 2018, 34, 15495−15506

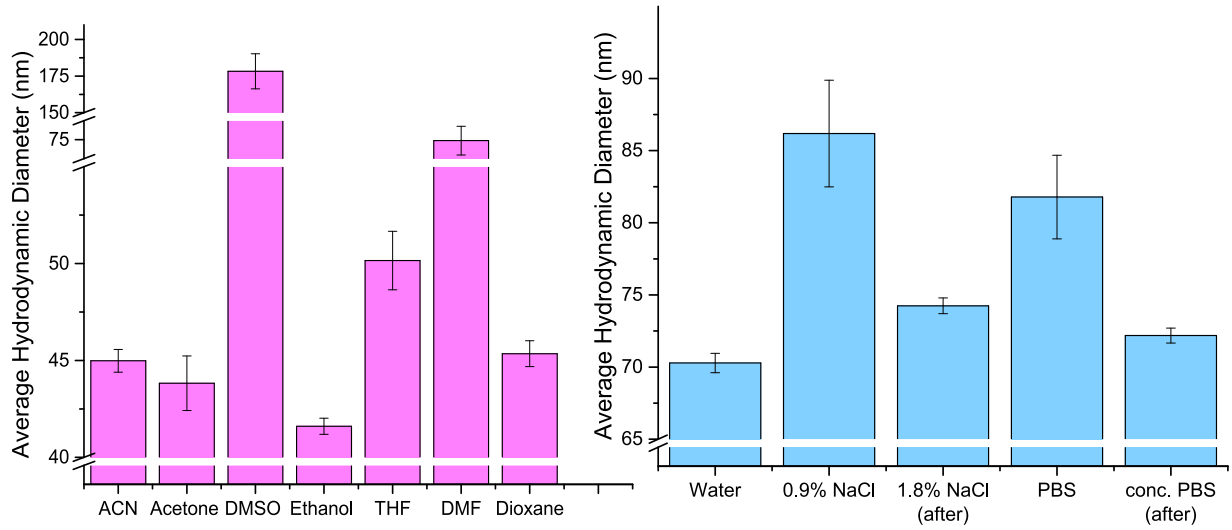

Figure 9. (Left) Effect of different solvents on the hydrodynamic diameter of $mPEG_{5k}$-*b*-p(HPMA-Bz)$_{18.5k}$ micelles. (Right) Effect of different aqueous phases on the hydrodynamic diameter of $mPEG_{5k}$-*b*-p(HPMA-Bz)$_{18.5k}$ micelles; in the graph, bars depicted with (after) were samples prepared in water and later concentrated solutions of salts were added (n = 3).

DMSO and DMF resulted in large micelles, 175 and 75 nm, respectively, compared to the micelles formed using THF, which were 50 nm. Acetone, acetonitrile, and dioxane resulted in smaller micelles of approximately 45 nm with polydispersities lower than 0.2. Generally, solvents with lower viscosity, such as THF, acetone, and acetonitrile, mix faster with water, which causes more uniform supersaturation, leading to smaller micelles.[71] On the other hand, solvents with relatively higher viscosity and surface tension (DMF and DMSO) have lower mixing rates with water, resulting in the growth of micelles and larger self-assemblies. In line with our observations, Kissel et al. reported that nanoparticles prepared using acetone were smaller than particles prepared in THF (140 and 180 nm, respectively) due to its lower viscosity and higher diffusion rate in water.[72]

The effect of the composition of the aqueous phase on the size of the obtained micelles was evaluated by addition of a 20 mg/mL polymer solution in THF to different aqueous phases. The micelles were slightly larger when they were made in either PBS or 0.9% NaCl solution (85 and 80 nm, respectively). Addition of salt to water increases the viscosity of the aqueous phase, which, in turn, affects the mixing of solvent and nonsolvent and thus nanoprecipitation of micelles in line with previous studies.[73] However, once the micelles were formed in water and the aqueous phase was subsequently adjusted by adding concentrated 1.8% NaCl solution or twice concentrated PBS, the size of micelles did not change (Figure 9), showing that the micellar structures are thermodynamically stable after formation.

CONCLUSIONS

The results of this study demonstrate that the self-assembly of mPEG-*b*-p(HPMA-Bz) polymers into micelles can be easily tailored in size. This size control relies on both the molecular weight of the polymers and the processing methods, which change the saturation conditions. In short, it can be said that reducing the micelle size can be accomplished by controlling the polymerization step and optimizing the polymer molecular weight by using higher hydrophilic-to-hydrophobic ratios. The size dependence coming from those ratios fits excellently into the de Gennes–Alexander theory and scaling law. Reducing the homopolymer content as a potential byproduct of block copolymer synthesis will also optimize the production of smaller micelles. Moreover, in terms of processing conditions, the use of organic solvents with faster mixing quality with water and applying higher rates of addition yield smaller and more homogenous micelles. This systematic study is of great importance as it indicates which parameters during the micelle formation process are critical to allow reproducible formation of micelles with a desired size. We are currently exploring these findings to develop a scalable route toward well-defined micelles for nanomedicine applications.

ASSOCIATED CONTENT

Supporting Information

The Supporting Information is available free of charge on the ACS Publications website at DOI: 10.1021/acs.langmuir.8b03576.

Detailed data on mPEG5k–ABCPA–mPEG5k macroinitiator, polymer and Micelle characterization, including the effect of different parameters on mPEG5k-b-p(HPMA-Bz)9.6k and mPEG5k-b-p(HPMA-Bz)4.7k polymers (PDF)

AUTHOR INFORMATION

Corresponding Author

*E-mail: W.E.Hennink@uu.nl.

ORCID

Olivier Sandre: 0000-0002-1815-2702
Cornelus F. van Nostrum: 0000-0003-4210-5241
Jan C. M. van Hest: 0000-0001-7973-2404
Wim E. Hennink: 0000-0002-5750-714X

Author Contributions

$^{\nabla}$M.B. and J.B. contributed equally to this work.

Author Contributions

All authors have given approval to the final version of the manuscript.

Notes

The authors declare no competing financial interest.

DOI: 10.1021/acs.langmuir.8b03576
Langmuir 2018, 34, 15495–15506

■ ACKNOWLEDGMENTS

The authors are grateful for the financial support received from the European Union's Horizon 2020 research and innovation program Marie Sklodowska-Curie Innovative Training Networks (ITN) under grant No. 676137 and HighTech Systems & Materials (HTSM) grant number 13312 from NWO.

■ REFERENCES

(1) Duncan, R.; Vicent, M. J. Polymer Therapeutics-Prospects for 21st Century: The End of the Beginning. *Adv. Drug Delivery Rev.* **2013**, *65*, 60−70.
(2) Hare, J. I.; Lammers, T.; Ashford, M. B.; Puri, S.; Storm, G.; Barry, S. T. Challenges and Strategies in Anti-Cancer Nanomedicine Development: An Industry Perspective. *Adv. Drug Delivery Rev.* **2017**, *108*, 25−38.
(3) Kunjachan, S.; Ehling, J.; Storm, G.; Kiessling, F.; Lammers, T. Noninvasive Imaging of Nanomedicines and Nanotheranostics: Principles, Progress, and Prospects. *Chem. Rev.* **2015**, *115*, 10907−10937.
(4) Björnmalm, M.; Thurecht, K. J.; Michael, M.; Scott, A. M.; Caruso, F. Bridging Bio-Nano Science and Cancer Nanomedicine. *ACS Nano* **2017**, *11*, 9594−9613.
(5) van Elk, M.; Murphy, B. P.; Eufrásio-da-Silva, T.; O'Reilly, D. P.; Vermonden, T.; Hennink, W. E.; Duffy, G. P.; Ruiz-Hernández, E. Nanomedicines for Advanced Cancer Treatments: Transitioning Towards Responsive Systems. *Int. J. Pharm.* **2016**, *515*, 132−164.
(6) Deng, C.; Jiang, Y.; Cheng, R.; Meng, F.; Zhong, Z. Biodegradable Polymeric Micelles for Targeted and Controlled Anticancer Drug Delivery: Promises, Progress and Prospects. *Nano Today* **2012**, *7*, 467−480.
(7) Mikhail, A. S.; Allen, C. Block Copolymer Micelles for Delivery of Cancer Therapy: Transport at the Whole Body, Tissue and Cellular Levels. *J. Controlled Release* **2009**, *138*, 214−223.
(8) Cabral, H.; Kataoka, K. Progress of Drug-Loaded Polymeric Micelles into Clinical Studies. *J. Controlled Release* **2014**, *190*, 465−476.
(9) Cagel, M.; Tesan, F. C.; Bernabeu, E.; Salgueiro, M. J.; Zubillaga, M. B.; Moretton, M. A.; Chiappetta, D. A. Polymeric Mixed Micelles as Nanomedicines: Achievements and Perspectives. *Eur. J. Pharm. Biopharm.* **2017**, *113*, 211−228.
(10) Houdaihed, L.; Evans, J. C.; Allen, C. Overcoming the Road Blocks: Advancement of Block Copolymer Micelles for Cancer Therapy in the Clinic. *Mol. Pharmaceutics* **2017**, *14*, 2503−2517.
(11) Varela-Moreira, A.; Shi, Y.; Fens, M. H. A. M.; Lammers, T.; Hennink, W. E.; Schiffelers, R. M. Clinical Application of Polymeric Micelles for the Treatment of Cancer. *Mater. Chem. Front.* **2017**, *1*, 1485−1501.
(12) Cabral, H.; Miyata, K.; Osada, K.; Kataoka, K. Block Copolymer Micelles in Nanomedicine Applications. *Chem. Rev.* **2018**, *118*, 6844−6892.
(13) Yuan, X.; Jiang, M.; Zhao, H.; Wang, M.; Zhao, Y.; Wu, C. Noncovalently Connected Polymeric Micelles in Aqueous Medium. *Langmuir* **2001**, *17*, 6122−6126.
(14) Shi, Y.; Lammers, T.; Storm, G.; Hennink, W. E. Physico-Chemical Strategies to Enhance Stability and Drug Retention of Polymeric Micelles for Tumor-Targeted Drug Delivery. *Macromol. Biosci.* **2017**, *17*, No. 1600160.
(15) Kang, N.; Perron, M.-È.; Prud'homme, R. E.; Zhang, Y.; Gaucher, G.; Leroux, J.-C. Stereocomplex Block Copolymer Micelles: Core−Shell Nanostructures with Enhanced Stability. *Nano Lett.* **2005**, *5*, 315−319.
(16) van Nostrum, C. F. Covalently Cross-Linked Amphiphilic Block Copolymer Micelles. *Soft Matter* **2011**, *7*, 3246−3259.
(17) Fang, J.; Nakamura, H.; Maeda, H. The EPR Effect: Unique Features of Tumor Blood Vessels for Drug Delivery, Factors Involved, and Limitations and Augmentation of the Effect. *Adv. Drug Delivery Rev.* **2011**, *63*, 136−151.
(18) Maeda, H.; Wu, J.; Sawa, T.; Matsumura, Y.; Hori, K. Tumor Vascular Permeability and the EPR Effect in Macromolecular Therapeutics: A Review. *J. Controlled Release* **2000**, *65*, 271−284.
(19) Torchilin, V. Tumor Delivery of Macromolecular Drugs Based on the EPR Effect. *Adv. Drug Delivery Rev.* **2011**, *63*, 131−135.
(20) Rizzo, L. Y.; Theek, B.; Storm, G.; Kiessling, F.; Lammers, T. Recent Progress in Nanomedicine: Therapeutic, Diagnostic and Theranostic Applications. *Curr. Opin. Biotechnol.* **2013**, *24*, 1159−1166.
(21) Bharali, D. J.; Mousa, S. A. Emerging Nanomedicines for Early Cancer Detection and Improved Treatment: Current Perspective and Future Promise. *Pharmacol. Ther.* **2010**, *128*, 324−335.
(22) Wang, J.; Mao, W.; Lock, L. L.; Tang, J.; Sui, M.; Sun, W.; Cui, H.; Xu, D.; Shen, Y. The Role of Micelle Size in Tumor Accumulation, Penetration, and Treatment. *ACS Nano* **2015**, *9*, 7195−7206.
(23) Cabral, H.; Matsumoto, Y.; Mizuno, K.; Chen, Q.; Murakami, M.; Kimura, M.; Terada, Y.; Kano, M. R.; Miyazono, K.; Uesaka, M.; Nishiyama, N.; Kataoka, K. Accumulation of Sub-100 Nm Polymeric Micelles in Poorly Permeable Tumours Depends on Size. *Nat. Nanotechnol.* **2011**, *6*, 815−823.
(24) Sun, Q.; Ojha, T.; Kiessling, F.; Lammers, T.; Shi, Y. Enhancing Tumor Penetration of Nanomedicines. *Biomacromolecules* **2017**, *18*, 1449−1459.
(25) Huang, K.; Ma, H.; Liu, J.; Huo, S.; Kumar, A.; Wei, T.; Zhang, X.; Jin, S.; Gan, Y.; Wang, P. C.; He, S.; Zhang, X.; Liang, X.-J. Size-Dependent Localization and Penetration of Ultrasmall Gold Nanoparticles in Cancer Cells, Multicellular Spheroids, and Tumors in Vivo. *ACS Nano* **2012**, *6*, 4483−4493.
(26) Dreher, M. R.; Liu, W.; Michelich, C. R.; Dewhirst, M. W.; Yuan, F.; Chilkoti, A. Tumor Vascular Permeability, Accumulation, and Penetration of Macromolecular Drug Carriers. *J. Natl. Cancer Inst.* **2006**, *98*, 335−344.
(27) Priwitaningrum, D. L.; Blondé, J.-B. G.; Sridhar, A.; van Baarlen, J.; Hennink, W. E.; Storm, G.; Le Gac, S.; Prakash, J. Tumor Stroma-Containing 3d Spheroid Arrays: A Tool to Study Nanoparticle Penetration. *J. Controlled Release* **2016**, *244*, 257−268.
(28) Shi, Y.; van der Meel, R.; Theek, B.; Oude Blenke, E.; Pieters, E. H. E.; Fens, M. H. A. M.; Ehling, J.; Schiffelers, R. M.; Storm, G.; van Nostrum, C. F.; Lammers, T.; Hennink, W. E. Complete Regression of Xenograft Tumors Upon Targeted Delivery of Paclitaxel Via Π−Π Stacking Stabilized Polymeric Micelles. *ACS Nano* **2015**, *9*, 3740−3752.
(29) Lo, C. L.; Lin, S. J.; Tsai, H. C.; Chan, W. H.; Tsai, C. H.; Cheng, C. H.; Hsiue, G. H. Mixed Micelle Systems Formed from Critical Micelle Concentration and Temperature-Sensitive Diblock Copolymers for Doxorubicin Delivery. *Biomaterials* **2009**, *30*, 3961−3970.
(30) Hu, Q.; Rijcken, C. J. F.; van Gaal, E.; Brundel, P.; Kostkova, H.; Etrych, T.; Weber, B.; Barz, M.; Kiessling, F.; Prakash, J.; Storm, G.; Hennink, W. E.; Lammers, T. Tailoring the Physicochemical Properties of Core-Crosslinked Polymeric Micelles for Pharmaceutical Applications. *J. Controlled Release* **2016**, *244*, 314−325.
(31) Talelli, M.; Rijcken, C. J. F.; Oliveira, S.; van der Meel, R.; van Bergen en Henegouwen, P. M. P.; Lammers, T.; van Nostrum, C. F.; Storm, G.; Hennink, W. E. Nanobody—Shell Functionalized Thermosensitive Core-Crosslinked Polymeric Micelles for Active Drug Targeting. *J. Controlled Release* **2011**, *151*, 183−192.
(32) De Vos, R.; Goethals, E. J. End Group Analysis of Commercial Poly(Ethylene Glycol) Monomethyl Ether's. *Polym. Bull.* **1986**, *15*, 547−549.
(33) Zimm, B. H. Apparatus and Methods for Measurement and Interpretation of the Angular Variation of Light Scattering; Preliminary Results on Polystyrene Solutions. *J. Chem. Phys.* **1948**, *16*, 1099−1116.
(34) Naksuriya, O.; Shi, Y.; van Nostrum, C. F.; Anuchapreeda, S.; Hennink, W. E.; Okonogi, S. Hpma-Based Polymeric Micelles for Curcumin Solubilization and Inhibition of Cancer Cell Growth. *Eur. J. Pharm. Biopharm.* **2015**, *94*, 501−512.

DOI: 10.1021/acs.langmuir.8b03576
Langmuir 2018, 34, 15495−15506

(35) Zhao, C. L.; Winnik, M. A.; Riess, G.; Croucher, M. D. Fluorescence Probe Techniques Used to Study Micelle Formation in Water-Soluble Block Copolymers. *Langmuir* **1990**, *6*, 514−516.
(36) Shi, Y.; van Steenbergen, M. J.; Teunissen, E. A.; Novo, Ls.; Gradmann, S.; Baldus, M.; van Nostrum, C. F.; Hennink, W. E. Π−Π Stacking Increases the Stability and Loading Capacity of Thermosensitive Polymeric Micelles for Chemotherapeutic Drugs. *Biomacromolecules* **2013**, *14*, 1826−1837.
(37) Neradovic, D.; van Nostrum, C. F.; Hennink, W. E. Thermoresponsive Polymeric Micelles with Controlled Instability Based on Hydrolytically Sensitive N-Isopropylacrylamide Copolymers. *Macromolecules* **2001**, *34*, 7589−7591.
(38) Hermanson, G. T. Zero-Length Crosslinkers. *Bioconjugate Techniques*, 3rd ed.; Academic Press: Boston, 2013; pp 259−273.
(39) Postma, A.; Davis, T. P.; Donovan, A. R.; Li, G.; Moad, G.; Mulder, R.; O'Shea, M. S. A Simple Method for Determining Protic End-Groups of Synthetic Polymers by 1h Nmr Spectroscopy. *Polymer* **2006**, *47*, 1899−1911.
(40) Su, W.-F. Radical Chain Polymerization. *Principles of Polymer Design and Synthesis*; Springer-Verlag: Berlin, Heidelberg, 2013; pp 137−183.
(41) Odian, G. Radical Chain Polymerization. *Principles of Polymerization*; John Wiley & Sons, Inc.: NJ, 2004; pp 198-349.
(42) Anonymous Ich Harmonised Guidelines, Impurities: Guideline for Residual Solvents Q3c(R6) Step 4.
(43) Ma, C.; Pan, P.; Shan, G.; Bao, Y.; Fujita, M.; Maeda, M. Core−Shell Structure, Biodegradation, and Drug Release Behavior of Poly(Lactic Acid)/Poly(Ethylene Glycol) Block Copolymer Micelles Tuned by Macromolecular Stereostructure. *Langmuir* **2015**, *31*, 1527−1536.
(44) Nie, T.; Zhao, Y.; Xie, Z.; Wu, C. Micellar Formation of Poly(Caprolactone-Block-Ethylene Oxide-Block- Caprolactone) and Its Enzymatic Biodegradation in Aqueous Dispersion. *Macromolecules* **2003**, *36*, 8825−8829.
(45) Nguyen, V. T. A.; De Pauw-Gillet, M.-C.; Sandre, O.; Gauthier, M. Biocompatible Polyion Complex Micelles Synthesized from Arborescent Polymers. *Langmuir* **2016**, *32*, 13482−13492.
(46) Giacomelli, C.; Schmidt, V.; Aissou, K.; Borsali, R. Block Copolymer Systems: From Single Chain to Self-Assembled Nanostructures. *Langmuir* **2010**, *26*, 15734−15744.
(47) Kale, T. S.; Klaikherd, A.; Popere, B.; Thayumanavan, S. Supramolecular Assemblies of Amphiphilic Homopolymers. *Langmuir* **2009**, *25*, 9660−9670.
(48) de Graaf, A. J.; Boere, K. W. M.; Kemmink, J.; Fokkink, R. G.; van Nostrum, C. F.; Rijkers, D. T. S.; van der Gucht, J.; Wienk, H.; Baldus, M.; Mastrobattista, E.; Vermonden, T.; Hennink, W. E. Looped Structure of Flowerlike Micelles Revealed by 1 h Nmr Relaxometry and Light Scattering. *Langmuir* **2011**, *27*, 9843−9848.
(49) Li, W.; Nakayama, M.; Akimoto, J.; Okano, T. Effect of Block Compositions of Amphiphilic Block Copolymers on the Physicochemical Properties of Polymeric Micelles. *Polymer* **2011**, *52*, 3783−3790.
(50) Soga, O.; van Nostrum, C. F.; Ramzi, A.; Visser, T.; Soulimani, F.; Frederik, P. M.; Bomans, P. H. H.; Hennink, W. E. Physicochemical Characterization of Degradable Thermosensitive Polymeric Micelles. *Langmuir* **2004**, *20*, 9388−9395.
(51) Li, Z.; Dormidontova, E. E. Kinetics of Diblock Copolymer Micellization by Dissipative Particle Dynamics. *Macromolecules* **2010**, *43*, 3521−3531.
(52) Sheng, Y.-J.; Wang, T.-Y.; Chen, W. M.; Tsao, H.-K. A−B Diblock Copolymer Micelles: Effects of Soluble-Block Length and Component Compatibility. *J. Phys. Chem. B* **2007**, *111*, 10938−10945.
(53) Williams, C.; Brochard, F.; Frisch, H. L. Polymer Collapse. *Annu. Rev. Phys. Chem.* **1981**, *32*, 433−451.
(54) Alexander, S. Adsorption of Chain Molecules with a Polar Head a Scaling Description. *J. Phys* **1977**, *38*, 983−987.
(55) de Gennes, P. G. Polymers at an Interface; a Simplified View. *Adv. Colloid Interface Sci.* **1987**, *27*, 189−209.
(56) de Gennes, P. G. Conformations of Polymers Attached to an Interface. *Macromolecules* **1980**, *13*, 1069−1075.
(57) Lee, H.; de Vries, A. H.; Marrink, S.-J.; Pastor, R. W. A Coarse-Grained Model for Polyethylene Oxide and Polyethylene Glycol: Conformation and Hydrodynamics. *J. Phys. Chem. B* **2009**, *113*, 13186−13194.
(58) Daoud, M.; Cotton, J. P. Star Shaped Polymers: A Model for the Conformation and Its Concentration Dependence. *J. Phys.* **1982**, *43*, 531−538.
(59) Mai, Y.; Eisenberg, A. Self-Assembly of Block Copolymers. *Chem. Soc. Rev.* **2012**, *41*, 5969−5985.
(60) Zhulina, E. B.; Adam, M.; LaRue, I.; Sheiko, S. S.; Rubinstein, M. Diblock Copolymer Micelles in a Dilute Solution. *Macromolecules* **2005**, *38*, 5330−5351.
(61) Astafieva, I.; Zhong, X. F.; Eisenberg, A. Critical Micellization Phenomena in Block Polyelectrolyte Solutions. *Macromolecules* **1993**, *26*, 7339−7352.
(62) Zhang, Z. G.; Yin, H. Effect of Polyoxypropylene Chain Length on the Critical Micelle Concentration of Propylene Oxide-Ethylene Oxide Block Copolymers. *J. Zhejiang Univ., Sci.* **2005**, *6*, 219−221.
(63) Torchilin, V. P. Structure and Design of Polymeric Surfactant-Based Drug Delivery Systems. *J. Controlled Release* **2001**, *73*, 137−172.
(64) Ashok, B.; Arleth, L.; Hjelm, R. P.; Rubinstein, I.; Onyuksel, H. In Vitro Characterization of Pegylated Phospholipid Micelles for Improved Drug Solubilization: Effects of Peg Chain Length and Pc Incorporation. *J. Pharm. Sci.* **2004**, *93*, 2476−2487.
(65) Makino, A.; Hara, E.; Hara, I.; Ozeki, E.; Kimura, S. Size Control of Core−Shell-Type Polymeric Micelle with a Nanometer Precision. *Langmuir* **2014**, *30*, 669−674.
(66) Zhang, C.; Pansare, V. J.; Prud'homme, R. K.; Priestley, R. D. Flash Nanoprecipitation of Polystyrene Nanoparticles. *Soft Matter* **2012**, *8*, 86−93.
(67) Caron, J.; Maksimenko, A.; Wack, S.; Lepeltier, E.; Bourgaux, C.; Morvan, E.; Leblanc, K.; Couvreur, P.; Desmaële, D. Improving the Antitumor Activity of Squalenoyl-Paclitaxel Conjugate Nanoassemblies by Manipulating the Linker between Paclitaxel and Squalene. *Adv. Healthcare Mater.* **2013**, *2*, 172−185.
(68) Aubry, J.; Ganachaud, F.; Cohen Addad, J. P.; Cabane, B. Nanoprecipitation of Polymethylmethacrylate by Solvent Shifting: 1. Boundaries. *Langmuir* **2009**, *25*, 1970−1979.
(69) Johnson, B. K.; Prud'homme, R. K. Mechanism for Rapid Self-Assembly of Block Copolymer Nanoparticles. *Phys. Rev. Lett.* **2003**, *91*, No. 118302.
(70) Aliabadi, H. M.; Elhasi, S.; Mahmud, A.; Gulamhusein, R.; Mahdipoor, P.; Lavasanifar, A. Encapsulation of Hydrophobic Drugs in Polymeric Micelles through Co-Solvent Evaporation: The Effect of Solvent Composition on Micellar Properties and Drug Loading. *Int. J. Pharm.* **2007**, *329*, 158−165.
(71) Lepeltier, E.; Bourgaux, C.; Couvreur, P. Nanoprecipitation and the "Ouzo Effect": Application to Drug Delivery Devices. *Adv. Drug Delivery Rev.* **2014**, *71*, 86−97.
(72) Beck-Broichsitter, M.; Rytting, E.; Lebhardt, T.; Wang, X.; Kissel, T. Preparation of Nanoparticles by Solvent Displacement for Drug Delivery: A Shift in the "Ouzo Region" Upon Drug Loading. *Eur. J. Pharm. Sci.* **2010**, *41*, 244−253.
(73) Huang, W.; Zhang, C. Tuning the Size of Poly(Lactic-Co-Glycolic Acid) (Plga) Nanoparticles Fabricated by Nanoprecipitation. *Biotechnol. J.* **2017**, *13*, No. 1700203.

DOI: 10.1021/acs.langmuir.8b03576
Langmuir 2018, 34, 15495−15506